Chemical Engineering Science 184 (2018) 273–284

Contents lists available at ScienceDirect

Chemical Engineering Science

journal homepage: www.elsevier.com/locate/ces

Fluid-structure interaction using lattice Boltzmann method: Moving boundary treatment and discussion of compressible effect

Wei Tan, Hao Wu, Guorui Zhu *

School of Chemical Engineering and Technology, Tianjin University, Tianjin 300350, China

HIGHLIGHTS

- A new moving boundary treatment based on BB method is proposed.
- FG method shows high reliability and stability in simulation.
- Vibration of cylinder in fluid is investigated using LBM.
- Compressible effect of LBM is investigated.

ARTICLE INFO

Article history:
Received 18 September 2017
Received in revised form 6 February 2018
Accepted 23 March 2018
Available online 26 March 2018

Keywords:
Lattice Boltzmann method
Fluid-structure interaction
Moving boundary treatment
Compressible effect
Vibration

ABSTRACT

We investigate fluid-structure interaction using lattice Boltzmann method (LBM), where we introduce a new simple treatment for moving boundary. Sub-grids are defined to separate structures from main-grid, thus structures can be created and calculated independently. Mapping and interpolation are used to connect main-grid and sub-grids. Our proposed simulation approach demonstrates high reliability and stability when compared to the direct bounce back method available in the literature. We validate the proposed approach by simulations of a single vibration cylinder in still water and in flowing water. The results show good agreement with theory and reference experiments. We find a delay of fluid force in the simulation of compact cylinder array, and conclude that Mach number (*Ma*) and boundary force term have a great influence on the accuracy of calculation results. *Ma* should be carefully chosen for a reliable result. Compressible effect in LBM and its influence on calculation of fluid-structure interaction, which has not been studied in detail, are also discussed in this paper. It is hard to avoid time delay effect under the framework of LBM according to the analysis, and this may lead to inaccurate results in fluid-structure interaction calculation using LBM under certain conditions, which deserve more attention. This paper investigates the vibration of structure in fluid using LBM, which will support the research for fluid induced vibration.

1. Introduction

Lattice Boltzmann method (LBM) has been developed into a promising numerical method for simulating complex flow problem due to its simplicity and efficiency. LBM, a method originated from Lattice Gas Cellular Automata (LGA) method (Frisch et al., 1986), is used to solve the macroscopic fluid dynamics based on a fully discrete Boltzmann kinetic equation at mesoscopic scale (Aidun and Clausen, 2010; Dawson et al., 1993; Chen and Doolen, 2012). The equation allows obtaining the pressure field and the stress tensor locally without solving any Poisson problem, which makes LBM very suitable for parallel computing. The method has been widely developed in fluid flow at a microscale, porous media, multiphase flow and many other fluid fields. As the study progressed, many problems arise in a larger scope of application, such as numerical instability problems (Ansumali and Karlin, 2000; Lallemand and Luo, 2000) especially at high Reynolds number flows. This disadvantage can be overcame using multiple-relaxation time (MRT) model (Luo et al., 2011; D'Humières, 2002; Lallemand and Luo, 2003). The relaxation parameters of MRT are represented by different physical quantities, such as fluid density, kinetic energy, momentum, energy flux and viscous stress tensor. These physical quantities can be relaxed to their respective equilibrium states by different relaxation times, which improve the flexibility of the algorithm. MRT can not only effectively eliminate fluctuations in velocity and pressure, but also greatly improve the numerical stability and accuracy of simulation. Due to the limitation of

* Corresponding author.
E-mail address: zhuguorui@tju.edu.cn (G. Zhu).

https://doi.org/10.1016/j.ces.2018.03.042
0009-2509/

calculation condition, the maximum allowed Reynolds number of single-relaxation time (SRT) is about 104 (Martínez et al., 1994).

Fluid-structure interaction is one of the most concerned fluid mechanics problems for computational fluid dynamic. Many researches have been devoted to these problems using LBM for the past two decades (Ladd, 1993; Filippova and Hänel, 1998; Mei et al., 1999; Bouzidi et al., 2001; Lallemand and Luo, 2003; Guo et al., 2002; AIAA, 2003; Hu et al., 2017; Peng et al., 2016; Ginzburg and D'Humières, 2003; Li et al., 2004; Mei et al., 2006; Caiazzo, 2013; Chen et al., 2014; Chen et al., 2013; Wu and Shu, 2009; Inamuro, 2012; De Rosis et al., 2014; De Rosis et al., 2014; Li et al., 2016; Wang et al., 2016; Delouei et al., 2016). The main challenge in the simulation of fluid-structure interaction using LBM is the treatment of moving boundary according to the transfer of distribution functions. Bounce Back (BB) method with moment correction was first proposed by Ladd (Ladd, 1993). This method has also been extended and improved to treat curved boundaries by many researches (Filippova and Hänel, 1998; Mei et al., 1999; Bouzidi et al., 2001; Lallemand and Luo, 2003; Guo et al., 2002; AIAA, 2003; Hu et al., 2017). Practical ways was provided to deal with moving boundary, but higher frequency fluctuations may be caused due to the movement of grid points in and out the region inside the solid structure. LBM combined with the immersed boundary method (IBM) (Wu and Shu, 2009; Inamuro, 2012; De Rosis et al., 2014; De Rosis et al., 2014; Li et al., 2016; Wang et al., 2016; Delouei et al., 2016) is widely used in most recent researches as it is based on the Cartesian grid which is suited for LBM. Although a lot of researches have been done regarding this topic and a number of cases have been confirmed, the reliability of LBM with moving boundary for complex situations, such as fluid-structure interaction cases involved close packed structures, needs further investigation.

This paper provides a new moving boundary method based on BB method (Mei et al., 1999), which is free from the problem of high frequency fluctuations. Cylinder vibration in still water and in flow water are simulated and the results are compared with theory and reference experiments. The compressible effect in fluid-structure interaction of Multi-structure using LBM is also discussed.

2. Lattice Boltzmann method

Instead of solving the Navier–Stokes (NS) equations directly, LBM is a mesoscopic method derived from the Boltzmann kinetic equation in a mesoscopic scale. The evolution equation (Chen and Doolen, 2012) is

$$|f(x_i + \boldsymbol{c}\delta_t, t_n + \delta_t)\rangle - |f(x_i, t_n)\rangle = |\Omega(\mathrm{x_i}, \mathrm{t_n})\rangle \tag{1}$$

where $|f(x_i, t_n)\rangle$ is the column vector of distribution function at position x_i and time t_n and $|f(x_i, t_n)\rangle \in \mathrm{V} \equiv \mathrm{R^Q}$, δ_t is the time step, c is the discrete velocity given by {(0, 0), (1, 0), (0, 1), (−1, 0), (0, −1), (1, 1), (−1, 1), (−1, −1), (1, −1)} for a D2Q9 model. $|\Omega(\mathrm{x_i}, \mathrm{t_n})\rangle$ is the discrete collision operator. We employ MRT model (Luo et al., 2011; D'Humières, 2002; Lallemand and Luo, 2003) to the function, in which the collision operator is:

$$|\Omega(\mathrm{x}, \mathrm{t})\rangle = -M^{-1} \cdot \hat{S} \cdot [|m\rangle - |m^{eq}\rangle] \tag{2}$$

$|m\rangle$ is the vector of moment can be denoted as:

$$|m\rangle = (\rho, e, \varepsilon, j_x, q_x, j_y, q_y, p_{xx}, p_{xy})^T \tag{3}$$

where ρ is the mass density, and $j_x = \rho u_x$ and $j_y = \rho u_y$ are x and y components of the flow momentum, respectively, which are the conserved moments in the system. Other moments are non-conserved moments and their equilibria are functions of the conserved moments in the system. For the vector of moment given above, the corresponding diagonal relaxation matrix of relaxation rates $\hat{S}$ is

$$\hat{S} = diag(s_\rho, s_e, s_\varepsilon, s_\chi, s_q, s_\chi, s_q, s_v, s_v) \tag{4}$$

3. Moving boundary condition

3.1. Conventional bounce back method

Moving boundary treatment is the core of fluid-structure interaction using LBM. Many researches have been performed for the treatment of curved boundary and moving boundary (Filippova and Hänel, 1998; Mei et al., 1999; Bouzidi et al., 2001; Lallemand and Luo, 2003; Guo et al., 2002; AIAA, 2003; Hu et al., 2017; Wu and Shu, 2009; Inamuro, 2012; De Rosis et al., 2014; De Rosis et al., 2014; Li et al., 2016; Wang et al., 2016; Delouei et al., 2016).

This paper mainly introduces a new improvement boundary treatment based on BB method. BB method considered a boundary lying between the solid and the fluid nodes denoted, respectively, by x_s and x_f as shown in Fig. 1. The physical boundary intersects the fluid-solid link between x_s and x_f at the point x_b. c_i and c_{-i} stand for directions opposite to each other, which are defined as $c_i = x_b - x_f$ and $c_{-i} = -c_i$, respectively. The lattice spacing is $\Delta x = 1$. The fraction of the intersected link in the fluid region is q, that is,

$$q = \frac{|x_f - x_b|}{|x_f - x_s|} = \frac{|x_f - x_b|}{\Delta x} \quad \text{with } 0 < q \leqslant 1 \tag{5}$$

After the collision step $f_i(x_f, t_n + \delta_t)$ is known after streaming from $x_{f'}$ as $\tilde{f}_i(x_{f'}, t_n)$. Where f and $\tilde{f}$ denote pre- and post-collision state of distribution function. $f_{-i}(x_f, t_n + \delta_t)$ is unknown and should be streamed from x_s as $\tilde{f}_{-i}(x_s, t_n)$ which is to be computed by following linear interpolation (Filippova and Hänel, 1998):

$$\tilde{f}_{-i}(x_s, t_n) = (1 - \chi)\tilde{f}_i(x_F, t_n) + \chi f_i^*(x_s, t_n) \tag{6}$$

where w_i is the weight factor corresponding to the i direction and u_w is the boundary velocity.

$f_i^*(x_s, t)$ is fiction distribution function and can be defined as:

$$f_i^*(x_s, t) = w_i \rho(x_F)\left[1 + \frac{3}{c^2}(c_i \cdot u_{SF}) + \frac{9}{2}\frac{(c_i \cdot u_{SF})^2}{c^4} - \frac{3}{2}\frac{u_F^2}{c^2}\right] \tag{7}$$

The value of u_{SF} and weighting factor χ can be obtained (Mei et al., 1999):

$$u_{SF} = \begin{cases} u_{SF} = u_{F'}, \quad \chi = \omega \cdot (2q - 1)/(1 - 2\omega), & q < 0.5 \\ u_{SF} = (1 - 3/2q) \cdot u_F + 3/2q \cdot u_w, \quad \chi = 2\omega \cdot (2q - 1)/(2 + \omega), & q \geqslant 0.5 \end{cases} \tag{8}$$

in which ω is the relaxation factor.

For a moving wall treatment using the BB scheme, a force term must be added to the bounced distribution function to reflect the

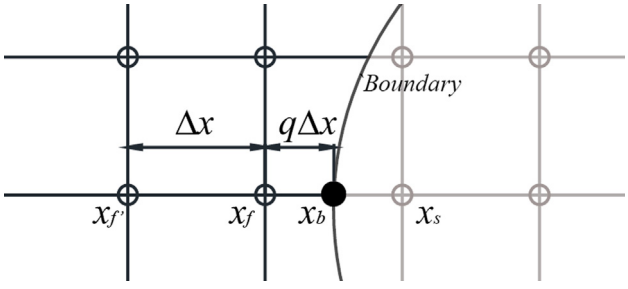

Fig. 1. Boundary conditions for a rigid wall intersect with link.

fluid structure interaction at the boundary surfaces. The distribution function should be formulated in the form as:

$$f_{-i}(r_s) = f_i(r_s) + 6w_i\frac{\rho}{c^2}(c_{-i}\cdot u_w) \tag{9}$$

3.2. New boundary treatment

The moving boundary method above may directly cause higher frequency fluctuations especially for fluid flow with curved boundary. This is caused by the moving in and out of grids which will change the boundary nodes numbers and the bounce back distribution functions all the time. To avoid this situation, a new treatment of moving boundary based on BB method is proposed in this paper. New moving boundaries are achieved by defining some extra floating grids (sub-grid) upon ordinary lattice (Main-grid). This method can be called Floating Grid method (FG) as sub-grids are floating upon main-grid.

3.3. Definition of sub-grid

Sub-grid is defined as shown in Fig. 2. Every sub-grid corresponds to a single structure. The size of sub-grid should be large enough to cover the structure. The definition of boundary nodes and solid nodes in sub-grid is the same as conventional BB method. Fluid nodes in the periphery of sub-grid need no operation. A local coordinate is defined for sub-grid corresponding to the movement of structure.

3.4. Coordinate transformation

Coordinate transformation is needed for the information exchange between sub-grid and main-grid. Here we define the local coordinate system of sub-grid as C_{sub} and the global coordinate system of main-grid as C_{main} Fig. 3)C_{sub} is a moving coordinate system and can be obtained as:

$$C_{sub}(t) = s_b(t) \tag{10}$$

where $s_b(t)$ is the displacement of boundary.

C_{main} is a stationary coordinate system. Coordinate transformation between sub-grid and main-grid is as follow:

$$X_{sub} + C_{sub} = X_{main} + C_{main} \tag{11}$$

where X_{sub} and X_{main} are the coordinates of same location in sub-grid and main-grid respectively.

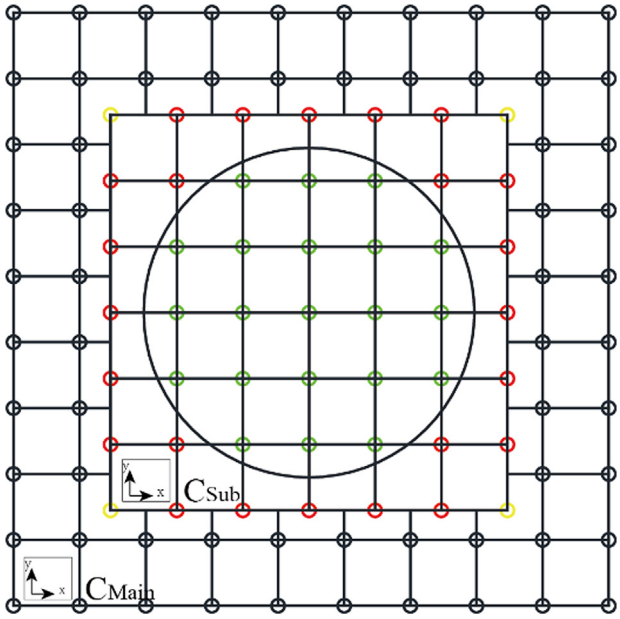

Fig. 3. Coordinate system of main-gird and sub-grid.

3.5. Information exchange between sub-grid and main-grid

As the nodes of sub-grid don't coincide with the nodes of main-grid, fiction nodes Fig. 4) are created to stream distribution function from main-grid to sub-grid. Supposing the coordinate of sub-grid's boundary node is $X_{boundary}$, the coordinate of fiction node can be obtained according to equation:

$$X_{ficiton} = X_{boundary} + c_{-i} + C_{sub} - C_{main} \tag{12}$$

The distribution functions of fiction node in i direction are interpolated by neighboring four main-grid nodes Fig. 4:

$$f_i(x_{fic}) = f_i(x_1)\cdot(1-s)(1-t) + f_i(x_2)\cdot s(1-t) + f_i(x_3)\cdot(1-s)t + f_i(x_4)\cdot s\cdot t \tag{13}$$

where s, t are x, y deviation values of fiction node relative to node 1 Fig. 4. Then $f_i(x_b)$ can be streamed from $f_i(x_{fic})$:

$$f_i(x_b, t_n + \delta_t) = f_i(x_{fic}, t_n) \tag{14}$$

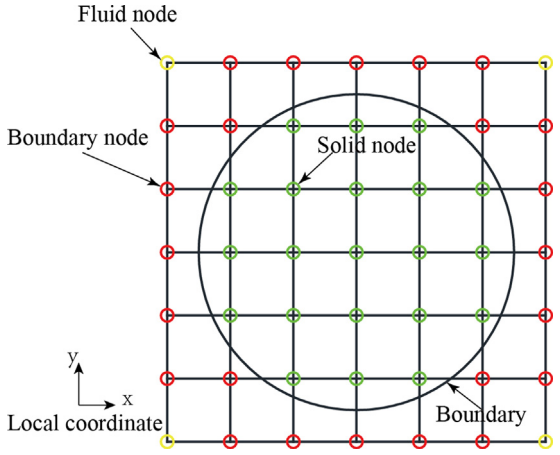

Fig. 2. Definition of sub-grid.

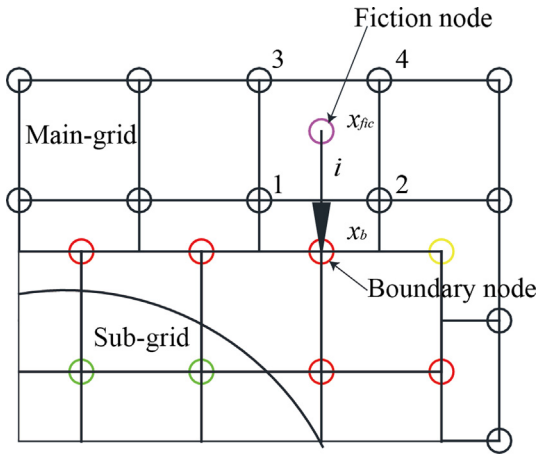

Fig. 4. Streaming from main-grid to sub-grid.

The value of sub-grid node is transported to main-grid node by mapping method. There are two main purposes for mapping operations. One is mapping the node states of sub-grid to main-grid nodes, the other is mapping the value of sub-grid nodes to the main-grid nodes.

Three types of node states are defined. Logical matrix B, S, F are defined for boundary nodes state, solid node state and fluid node state respectively, where $\sim F = (B \vee S)$. The node states of sub-grid are mapped to main-grid by preforming logical operations on neighboring four sub-grid nodes Fig. 5):

Boundary node: $B_j^{Main} = \sim \left(F_k^{Sub} \wedge F_{k+1}^{Sub} \wedge F_{k+2}^{Sub} \wedge F_{k+3}^{Sub}\right) \wedge \sim \left(S_k^{Sub} \wedge S_{k+1}^{Sub} \wedge S_{k+2}^{Sub} \wedge S_{k+3}^{Sub}\right)$

Solid node: $S_j^{Main} = S_k^{Sub} \wedge S_{k+1}^{Sub} \wedge S_{k+2}^{Sub} \wedge S_{k+3}^{Sub}$

$$\text{Fluid node}: F_j^{Main} = \sim (B_j^{Main} \wedge S_j^{Main}) \tag{15}$$

It can be inferred from Fig. 6 that the main-grid nodes nearest to the boundary are set as boundary nodes by Eq. (15). Some boundary nodes may locate inside the boundary. This is a little different from the conventional BB method.

The distribution functions of main-grid boundary node need to be determined by surround sub-grid boundary nodes. The distribution function of main-grid boundary node can be obtained by:

$$f_i^{Main\_B} = f_i^{interp} + \sum \delta(r) \cdot f_i^{ex\_Sub} \tag{16}$$

where f_i^{interp} is interpolated by surrounding four sub-grid nodes without using Eq. (9):

$$f_i(x_j) = f_i(x_k) \cdot (1-s)(1-t) + f_i(x_{k+1}) \cdot s(1-t) + f_i(x_{k+2}) \cdot (1-s)t + f_i(x_{k+3}) \cdot s \cdot t \tag{17}$$

where s, t are x, y deviation values of node j relating to node k Fig. 5. Equilibrium distribution functions computed according to the boundary velocity are used for solid nodes. $f_i^{ex\_Sub}$ is the force term in Eq. (9). $\delta(r)$ is a smoothed four-point delta function (Yang et al., 2009) as below:

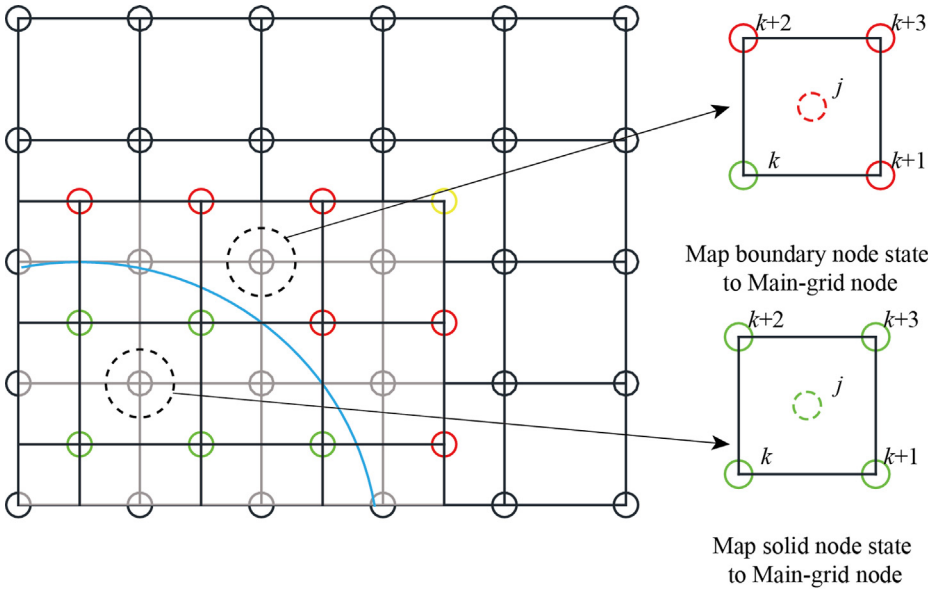

Fig. 5. Mapping criterion.

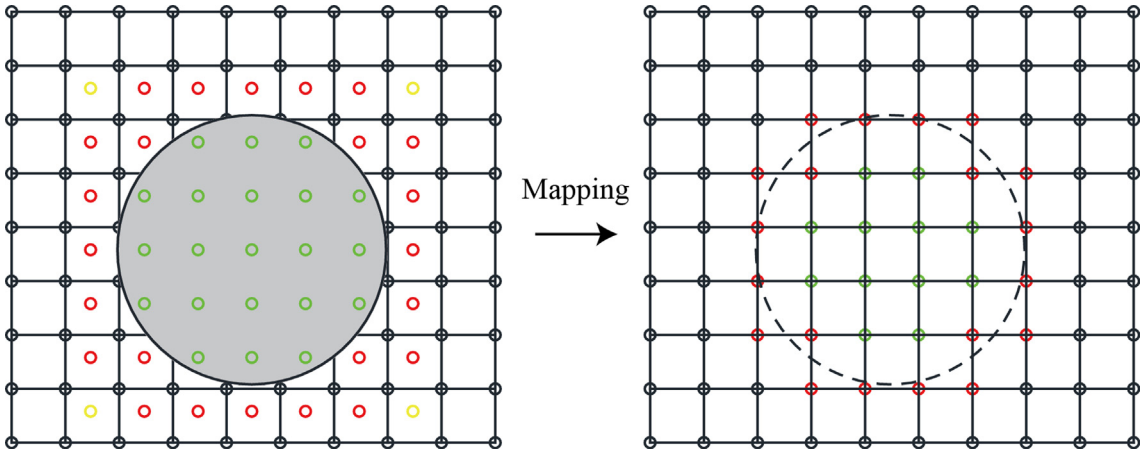

Fig. 6. Mapping sub-grid node states to main-grid nodes.

$$\delta(r)=\begin{cases}\frac{3}{8}+\frac{\pi}{32}-\frac{r^2}{4}, & |r|\leqslant 0.5\\ \frac{1}{4}+\frac{1-|r|}{8}\sqrt{-2+8|r|-4r^2}-\frac{1}{8}\arcsin(\sqrt{2}(|r|-1)), & 0.5\leqslant|r|\leqslant 1.5\\ \frac{17}{16}-\frac{\pi}{64}-\frac{3|r|}{8}+\frac{r^2}{8}+\frac{|r|-2}{8}\sqrt{-14+16|r|-4r^2} & \\ +\frac{1}{16}\arcsin(\sqrt{2}(|r|-2)), & 1.5\leqslant|r|\leqslant 2.5\\ 0 & |r|\geqslant 2.5\end{cases} \tag{18}$$

where r is the distance between the main-grid boundary node and the sub-grid boundary nodes. Thus the boundary forces are distributed smoothly to the main-grid boundary nodes around and the fluctuation can be decreased by this method.

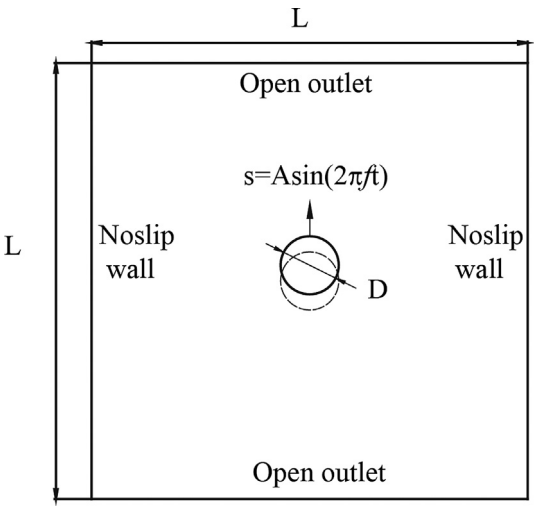

Fig. 7. A cylinder vibration in still water.

Table 1
Simulations in different grid number.

Case	Lattice number in diameter	*Cm* (BB-method)	*Cm* (FG-method)
A	30	1.2875	1.035
B	60	1.2455	1.004
C	120	1.235	0.995

The implementation process of this method is as follows:

(a) Collision step for main-grid and sub-grids;
(b) Streaming step for main-grid, where only fluid nodes need to be streamed;
(c) Stream from main-grid to sub-grids. Fiction nodes are created by interpolation. Only boundary nodes in sub-grids need to be streamed.
(d) Compute the displacement and velocity of structures and update the coordinates of sub-grids;
(e) Map sub-grids to main-grid.

Hydrodynamic evaluation is another important issue for fluid structure interaction. Momentum exchange method is a convenient and stable way for force evaluation and different Momentum exchange methods have been detailed researched by former researches (Tao et al., 2016), Wen's method (Wen et al., 2014) is adopted in this paper.

4. Simulation

4.1. Single cylinder vibration in still water

Firstly, we conduct a simulation about the moving boundary to compare the conventional BB method and FG method raised in this paper. The geometry of boundary conditions is shown in Fig. 7. The domain fluid field is 0.2 m ∗ 0.2 m. The left and right boundaries are set as no-slip wall with half bounce method, and the top and bottom boundaries are defined as open outlets with characteristic nonreflecting boundary conditions (Izquierdo and Fueyo, 2008). Cylinder in the center of the domain fluid field vibrates sinusoidally in y direction with $y(t) = \mathrm{Asin}(2\pi ft)$, and the diameter of cylinder is $D = 0.03$ m. Here, A is set as $0.1D$, and f is equal to 5 Hz. The fluid is water with $\mu = 0.001$ Pa·s and $\rho = 1000$ kg/m^3. Mach number $Ma = V_{max}/c_s$ is selected as 0.01 in this simulation. The non-dimensional force coefficient C_m can be calculated by $F_{fluid}/(4Af^2\rho\pi^3D^2/4)$, in which F_{fluid} is the fluid force of cylinder. Simulations with different grid numbers are shown in Table 1, the result of case C is used for analysis.

Comparison results of C_m with two boundary methods are shown in Table 1 and Fig. 7. C_m from BB method is about 1.24 time of that with FG method. As theoretical value of $C_m = 1$ (Chen, 1987) for small amplitude vibration, BB method's result is overestimated. This may cause the overestimation of force when q deviates 0.5

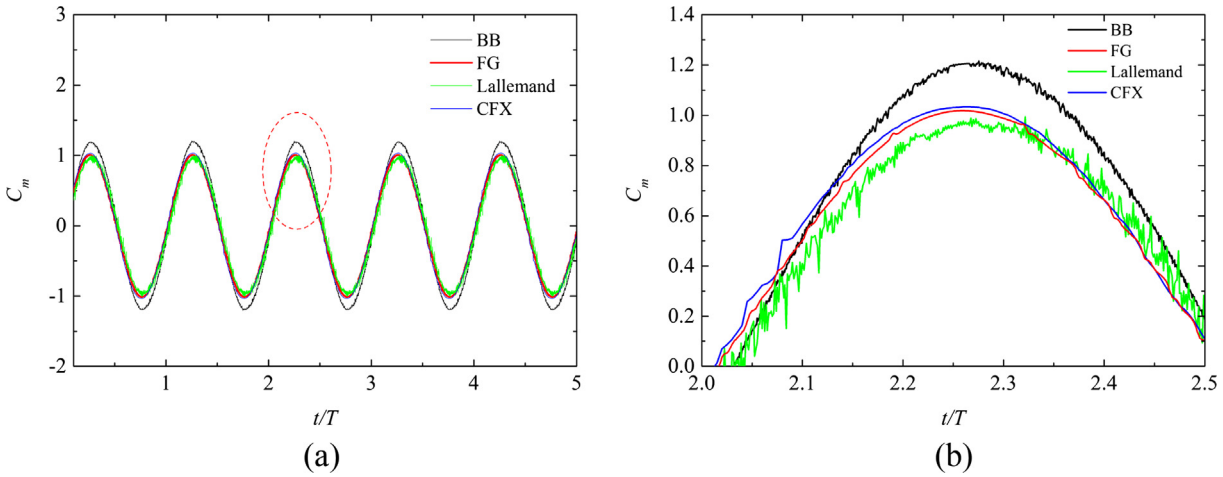

Fig. 8. Comparison of C_m using different method. (a) Over all view, (b) Local view.

using Eq. (9). As FG method uses Eq. (10) to spread force term, the average operation in some extent reduces the force term, and this is where the difference comes from. Pierre Lallemand and Li-Shi Luo (Lallemand and Luo, 2003) revised the force term for q > 0.5 with dividing force term by $q(2q + 1)$. Result of Lallemand's method can be seen in Fig. 8, which is close to the result of FG. Result of CFX software is also presented in Fig. 8, and shows a good agreement with FG. It is verified the result of FG. The configuration of CFX is refer to (Hassan et al., 2009).

As can be seen in Fig. 8 (b), FG method shows smooth results, while the results from BB method have a lot of fluctuations. It can be concluded that FG method has a better stability than BB method.

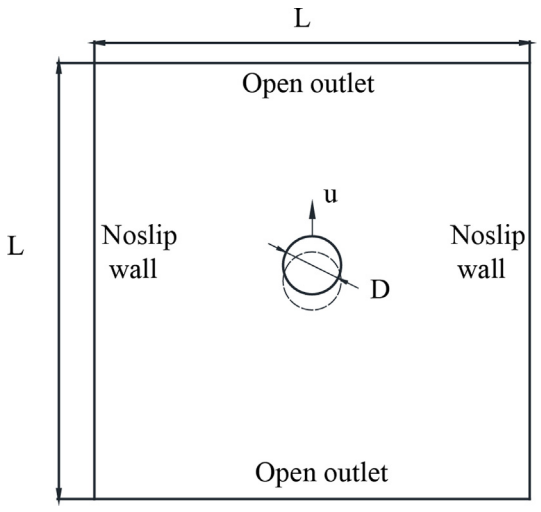

Fig. 9. Free vibration of a cylinder in still water.

Table 2
Simulations in different grid number.

Case	Lattice number in diameter	*Y/D*
A	30	0.098
B	60	0.0965
C	120	0.0959

4.2. Free decay vibration of a cylinder in still water

The boundary of model is shown in Fig. 9. The size of domain is 0.2 m ∗ 0.2 m. The viscosity and density of fluid are $\mu = 0.001$ Pa·s and $\rho = 1000$ kg/m^3. Here we set stiffness and the mass of cylinder as $k = 1184.38$ N/m and $m = 1.2$ kg, respectively, which gives a natural frequency of 5 Hz in vacuum. An initial velocity of u = 0.1 m/s is given to the cylinder in y direction which makes it freely vibrate in fluid.

Simulation results of different gird size are compared in Table 2. As the calculation is unstable at the very beginning of simulation, *Y/D* at second peak is used for comparison, where *Y* is the displacement of cylinder in y direction. Result of case C is used for analysis.

For cylinder freely vibrate in still water, it suffers the inertial force and viscous force of fluid, and the motion of cylinder will decay in time. Natural frequency of cylinder is reduced due to the added mass of heavy fluid. The theory ratio of natural frequency in water to natural frequency in vacuum can be calculated as $f_{water}/f_{vacum} = \sqrt{\frac{m}{m+\rho\pi D^2/4}} = 0.8$ (Chen and Chung, 1976).

Significant amplitude decay and decrease in frequency can be seen in Fig. 10. The results of CFX method are presented for comparison. The results match well between FG method and CFX method. A frequencies ratio of 0.794 and 0.788 can be obtained from FG and CFX method respectively, which is consistent with the theory value of 0.8.

4.3. Vortex induced oscillation of a cylinder

Vortex induced oscillation of a cylinder is a classic problem of fluid-structure interaction with plenty of numerical and experimental studies (Anagnostopoulos and Bearman, 1992; Mittal and Tezduyar, 2010; Takashi et al., 1992; Takashi, 1994; Blevins and Saunders, 1977; Dettmer and Perić, 2006; Roshko, 1954). The experiment of (Anagnostopoulos and Bearman, 1992) is used to verify the simulation in this paper. The geometry and the boundary conditions employed in the simulation are displayed in Fig. 11. The parameters of this simulation refer to (Dettmer and Perić, 2006). The spring is linear with the stiffness $k = 5.79$ N/m and damping factor $c = 0.325$ g/s. The mass and the diameter of the cylinder are given as $m = 2.979$ g and $D = 0.16$ cm, respectively. Thus, the natural frequency of the cylinder follows as $f_n = 7.016$ Hz. The fluid under consideration is water with $\mu = 0.01$ g/(cm s) and $\rho = 1.0$ g/cm^3. The Reynolds number $Re = \rho Du/\mu$ varies between 90 and 140. The

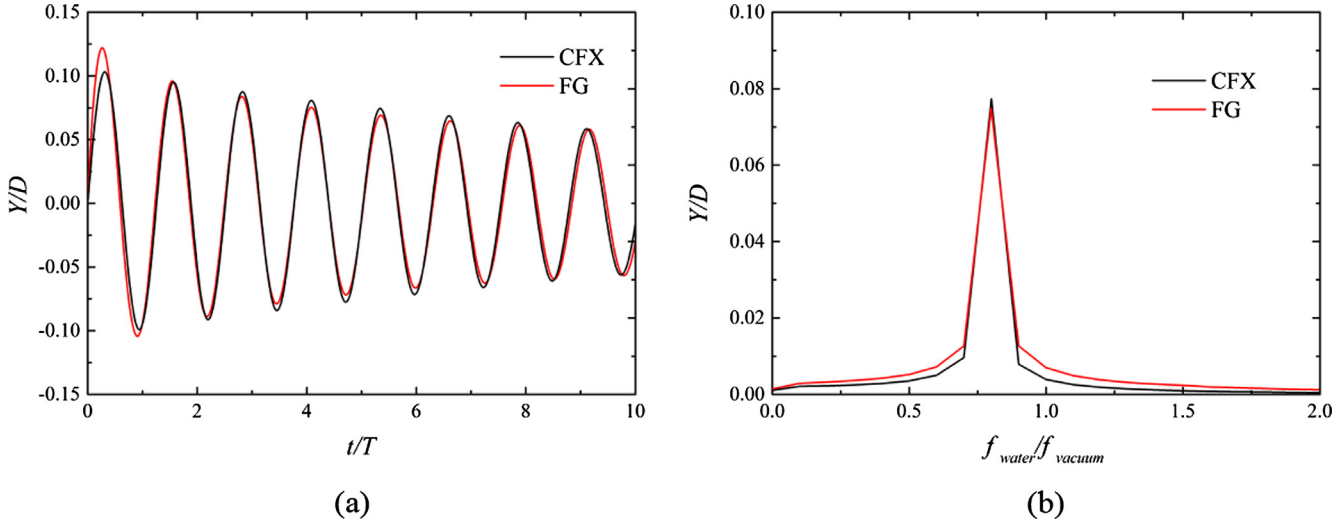

Fig. 10. Decay of free vibration. (a) Time history, (b) Spectrum.

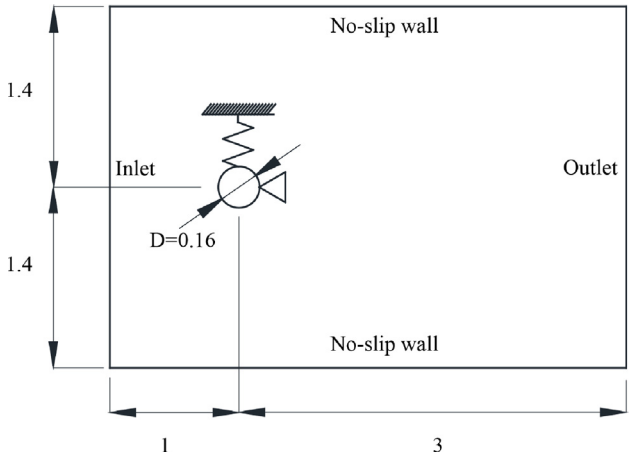

Fig. 11. Geometry ([cm]) and boundary conditions.

Mach number is $Ma = V_{inlet}/c_s = 0.02$. Both stationary cylinder simulaiton(short as SCS) and moving cylinder simulation(short as MCS) are conducted in this paper.

Grid sizes of 1250×875, 2500×1750, 3750×2625 are used to discuss grid independency of the model, which gives lattice number of 50,100,150 in diameter respectively. Lift force coefficients (C_f) at $Re = 140$ are compared for SCS, and $Y/Ds.$ at Re = 102 (lock-in region) are compared for MCS. It can be seen in Table 3. Three grid sizes are all capable for simulation. The model of case A are used for simulation for time saving.

The comparison of SCS, MCS and experiment results is shown in Fig. 12. f_v is shedding frequency and f_n is natural frequency of cylinder. The results are almost completely coincident with the curve proposed by Roshko (Roshko, 1954) which indicates high reliability of SCS with FG method in this paper. In addition, the results of MCS clearly show a lock-in region, which is explained as follows. f_v/f_n of MCS is coincident with that of SCS at $Re < 98$, and jumps to 1 at $Re = 98$, then stays the same until about $Re = 108$, after which the ratio is again coincident with that of SCS. These points of MCS and the trend are also compared with the experiment (Anagnostopoulos and Bearman, 1992) and both show good agreement with the experiment.

Amplitude comparison between simulation and experiment is shown in Fig. 13. It is obvious that simulation result has the same trend with the experimental measurement while the values have some deviations. The maximum amplitudes by simulation is 21%

Table 3
Simulations in different grid number.

Case	Lattice number in diameter	C_f for SCS	Y/D for MSC
A	50	0.280	0.356
B	100	0.278	0.353
C	150	0.277	0.353

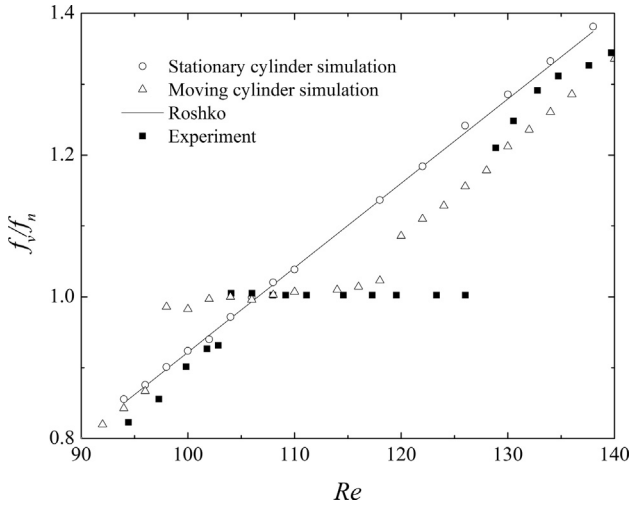

Fig. 12. Shedding frequency comparison between simulations and experiment.

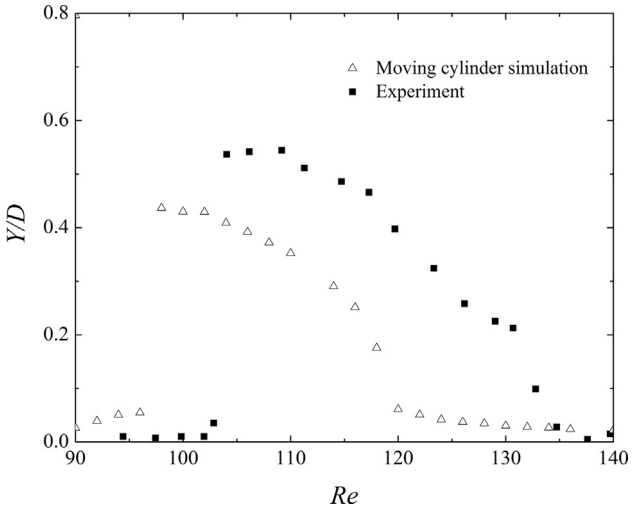

Fig. 13. Amplitude comparison between simulation and experiment.

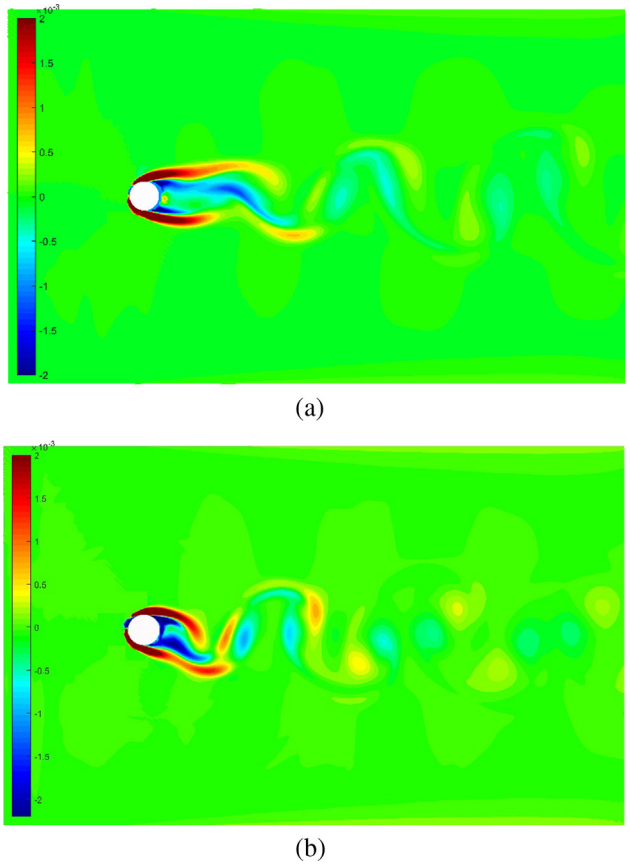

Fig. 14. Evolution of vortex at $Re = 104$, (a) $t/T = 7$ (b) $t/T = 28$.

larger than the experimental values and the start of lock-in region is a little earlier than that of experiment. This may due to some significant differences between the numerical and experimental models. In the experiment, the submerged length of the cylinder and the depth of the water channel are 12 cm and 70 cm, respectively. The flow involves a free surface on the tip of cylinder, which may cause aggressive results.

Evolution of the lock-in effect is displayed in Figs. 14 and 15. Shedding frequency synchronizes to natural frequency of cylinder when they are close Fig. 14. Beat vibration can be seen before

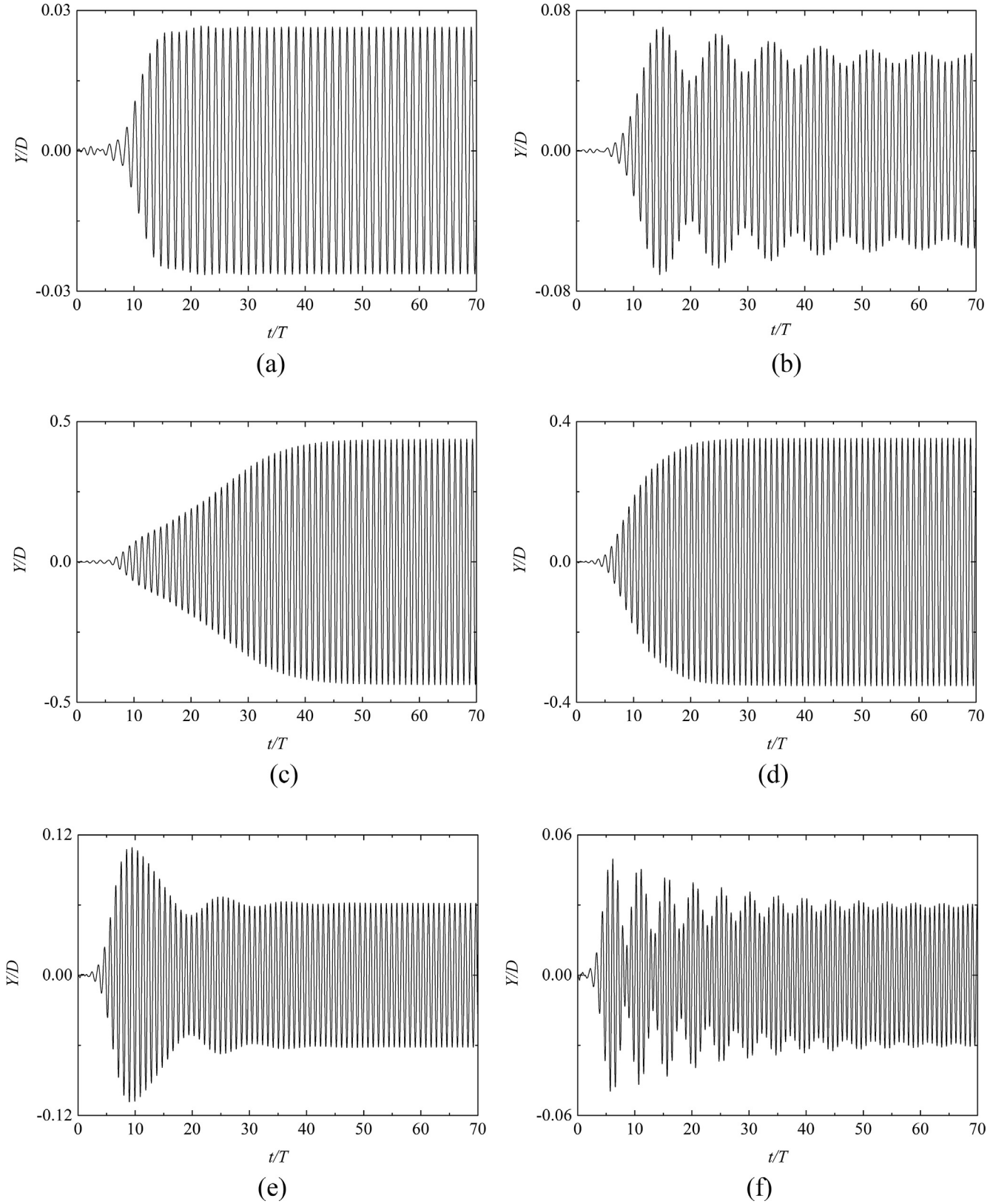

Fig. 15. Evolution of the amplitudes of the cylinder oscillation at different *Re*. (a) *Re* = 90, (b) *Re* = 96, (c) *Re* = 98, (d) *Re* = 102, (e) *Re* = 120, (f) *Re* = 130.

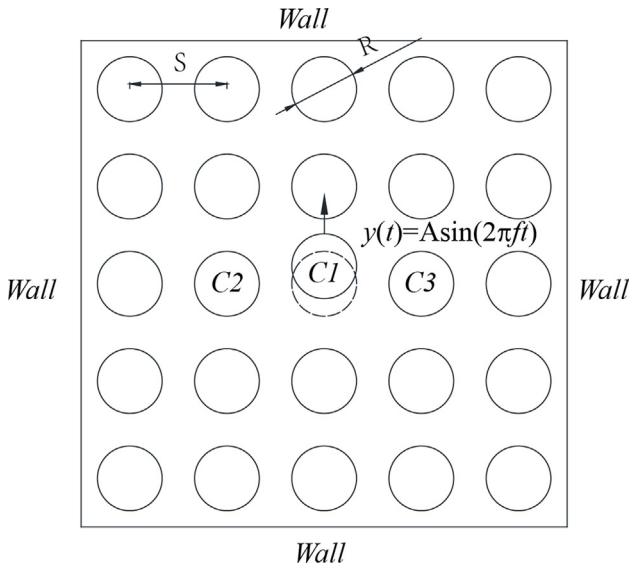

Fig. 16. Geometry and boundary conditions of cylinder array.

Table 4
Simulations in different grid number.

Case	Lattice number in diameter	Cm
A	30	1.270
B	60	1.246
C	120	1.241

and after the lock-in region Fig. 15(b, f)). As the lock-in region comes to an end, oscillation starts with a sudden jump Fig. 15(e)). As the Reynolds number increases, the amplitude of the oscillations smoothly decreases to a much gentle state Fig. 15(f)). In general, the simulation results of this paper are convincingly compared with the former experiment.

4.4. A cylinder vibration in cylinder array in still water and discussion of compressible effect

Tube vibration in a tube array is a typical application of multi-structure interaction. This has been intensively studied by many researchers, including experimental and theoretical (Chen, 1987; Chen and Chung, 1976; Tanaka et al., 2002). Cylinder and cylinders around it are subjected to inertial force due to its own vibration. The geometry of simulation is displayed in Fig. 16. A 5 × 5 cylinder array is built, with a pitch of $S = 0.04$ m and a diameter of $D = 0.03$ m, and the full size of fluid domain is 0.2 m × 0.2 m with wall around it. The fluid under consideration is water with $\rho = 1000\ \mathrm{kg/m^3}$ and $\mu = 10^{-3}$ Pa s. The center cylinder oscillates sinusoidally in y direction with $y(t) = \mathrm{Asin}(2\pi ft)$. We set $\mathrm{A} = 0.1D = 0.003$ m in simulation. Three grid dimensions are adopted for grid independency analysis. They are dimensions of 401 × 401, 801 × 801 and 1601 × 1601, which are usedto ensure that at least 30, 60, 120 nodes are covered in a length of D respectively. The non-dimensional force coefficient can be expressed as $C_m = \mathrm{F_{fluid}}/(\mathrm{A}\omega^2\rho\pi D^2/4)$. C_m of center tube at $Ma = 0.01$ for different grids are shown in Table 4 Here case B is used for simulation considering accuracy and time saving.

Different Mach number $Ma = 0.05$, 0.01, 0.005, 0.0025 are chosen to take compressible effect of LBM into consideration.

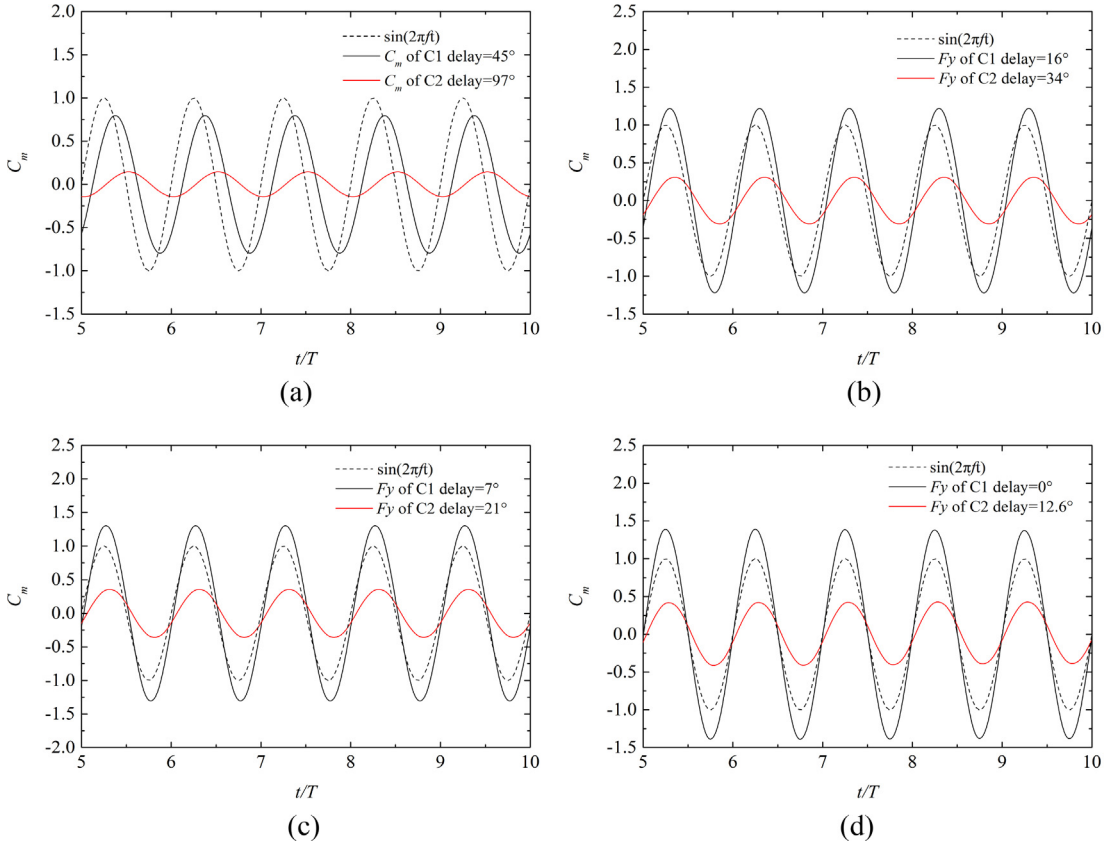

Fig. 17. C_m of C1, C2 due to motion of C1 as a function of time, (a) $Ma = 0.05$, (b) $Ma = 0.01$, (c) $Ma = 0.005$, (d) $Ma = 0.0025$.

Theoretically speaking, the fluid forces of C1, C2, C3 are in phase with the motion of C1, and C2 is identical to C3 due to symmetry. Thus, only forces of C1 and C2 are analyzed.

4.4.1. Phase lag analysis

The time history of C_m of C1 and C2 induced by the motion of C1 with different *Ma* are shown in Fig. 17. Distinguished from theoretical results, a phase lag arises between the fluid forces of C1, C2 and the motion of C1, which means the effect of C1's motion on C1 and C2 is delayed in time. Phase lag decreases with the decrease of *Ma*.

4.4.2. Amplitude analysis

C_m of C1 and C_m of C2 at different *Ma* are compared with the experiment of Tanaka (Tanaka et al., 2002). According to Table 5, with the decrease of *Ma*, prediction of fluid forces coefficient changes from underestimation to overestimation compared with experment result.

4.4.3. Discussion of the results

As can be seen in Fig. 17 and Table 5, with the decrease of *Ma*, the phase lag decreases and the C_m increases. Reasonable results can be obtained only for *Ma* around 0.01 in this case. Fluid forces increase with the decrease of *Ma*, which is caused by the strong transient effect of cylinder vibration and the compressible effect of LBM.

Fig. 18 shows a simplified illustration of LBM transportation in time. Particle 1 is supposed to have a velocity *U* at time *t*, and it will influence particle 3 after a moment of $2\Delta t$ by streaming and collision step, while the changing from state of Fig. 18(a) to state of Fig. 18(c) is almost instantaneous for real incompressible flow. This time lag is inevitable under the scheme of LBM. In steady state or weak transient state analysis, the time cost for state change is much larger than Δt, thus they are not sensitive to Δt. Due to the reasons above, there will be enough time for steady state and weak transient state to iterate to an expected state. But for strong transient cases, things will be different. One choice of remedy for strong transient analysis is to reduceΔt, which also means to reduce *Ma* in LBM simulation.

Table 5
Comparison of C_m between experiment and simulation.

Mach number	C_m of C1 (error)	C_m of C2(error)
Experiment Tanaka et al. (2002)	1.28	0.33
0.05	0.814(−36.4%)	0.149(−55.0%)
0.01	1.246(−2.7%)	0.316(−4.2%)
0.005	1.332(4.1%)	0.365(10.5%)
0.0025	1.421(11.0%)	0.428(29.7%)

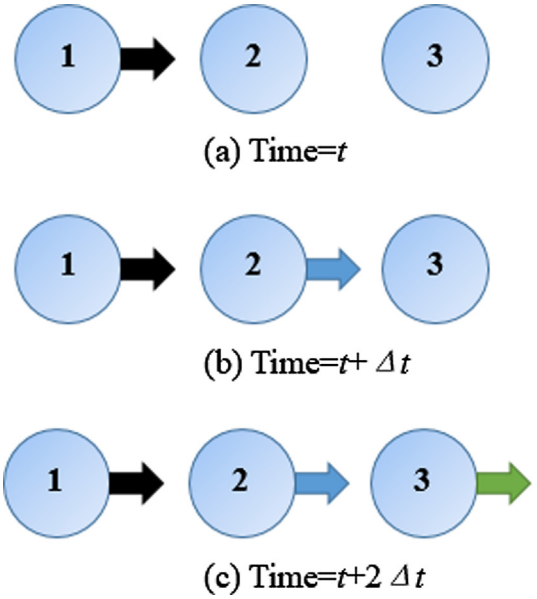

Fig. 18. Transport of particle in one dimention.

Cylinder vibration in water is a strong transient case and the velocity of boundary and fluid surround changes dramatically from time to time. The vectors of velocity around oscillation cylinder for *Ma* = 0.05 and *Ma* = 0.0025 at different times are demonstrated in Fig. 19. Δt for *Ma* = 0.05 is about 20 times that of *Ma* = 0.0025. For cylinder moves in real incompressible fluid, flow pattern can be described as follow:

(a) Cylinder starts to move from static, and flow circulation around cylinder is formed instantly.
(b) Cylinder moves in acceleration and flow circulation also accelerates.
(c) Cylinder moves in deceleration and flow circulation also decelerates.
(d) Cylinder stops moving and flow settles down.

Results of *Ma* = 0.0025 Fig. 19(b, d, f, h)) show a good agreement of this pattern, corresponding to the small phase lag of C1. As a comparsion, the motion of cylinder is much faster than the distribution of flow at a *Ma* = 0.05 Fig. 19(a, c, e, g)), which is corresponding to the rather large phase lag of C1.

Similar situation can be applied to adjacent cylinders, and the time delay effect for adjacent cylinders is severer. The flow resulting from the moving cylinder just reaches adjacent cylinder at t = 0.001 s and *Ma* = 0.0025 Fig. 19(b)), and a fully developed circulation is formed later at about 0.007 s, which corresponds to the phase lag of C2 in Fig. 17(d).

Although small *Ma* orΔt can reduce the time delay caused by transfer sheme of LBM, smallΔt aggravates the fluid force Table 5due to the use of Eq. (9) with the reduce of *Ma*. Besides, the influence of force term in Eq. (9) increases with the decrease of *Ma*. Considering the extreme caseΔt approaching to 0, the present of force term can be taken as an inlet boundary, while this is incorrect in fact. A balance between compressible effect of LBM and moving boundary is needed to be considered and different *Ma* should be chosen for different cases. For example, only a relatively reasonable result can be obtained in above case at *Ma* = 0.005–0.01.

According to the analysis above, fluid-structure interaction using LBM in some situations may not be accurated due to the compressible effect of LBM and moving boundary using Eq. (9). This needs attentions espacially for cases involving multi-structure interaction.

5. Conclusion

Fluid-structure interaction using LBM is discussed in this paper, and a new moving boundary treatment is proposed to reduce the unexpected fluctuations and to improve the stablity in the simulation of flow around moving boundary. Simulations for a cylinder in still water and in flow water are processed and show good agreements with theory and experiment, which verifies the reliablity of the new moving boundary treatment. The compressible effect in fluid-structure interaction using LBM is also discussed. Simulations of cylinder array in this paper reveal that compressible effect and moving boundary force term has a significant influence on the numerical accuracy for multi-structure interaction case, and *Ma* should be carefully chosen for a reliable result.

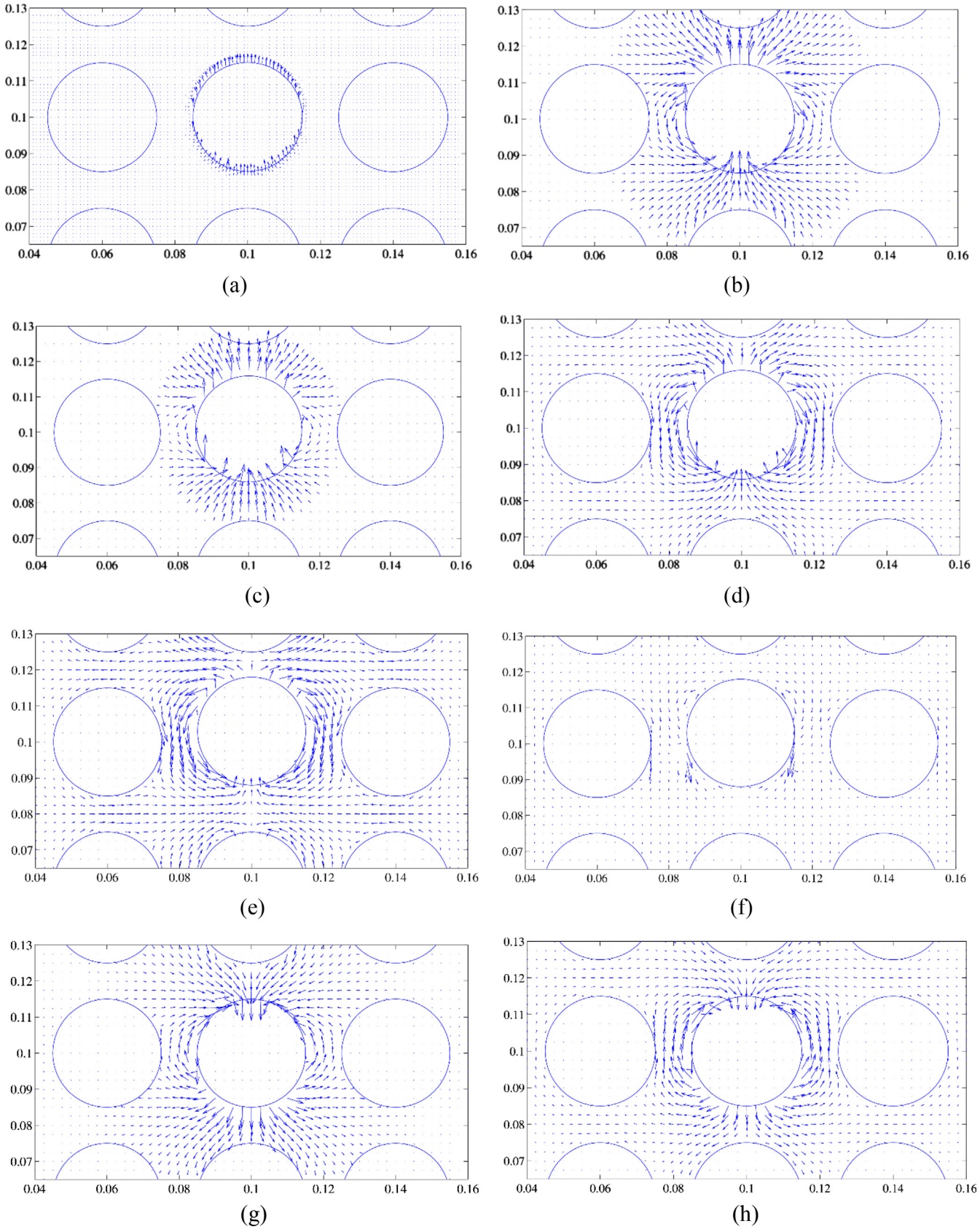

Fig. 19. vector of velocity for Ma = 0.05 and 0.0025 at different time. (a) Ma = 0.05 t/T = 0.005, (b) Ma = 0.0025 t/T = 0.005, (c) Ma = 0.05 t/T = 0.05, (d) Ma = 0.0025 t/T = 0.05, (e) Ma = 0.05 t/T = 0.25, (f) Ma = 0.0025 t/T = 0.25, (g) Ma = 0.05 t/T = 0.5, (h) Ma = 0.0025 t/T = 0.5.

Acknowledgements

This work is supported by the Natural Science Foundation of China (21606164).

References

AIAA, 2003. A unified boundary treatment in lattice Boltzmann method. In: APS Division of Fluid Dynamics Meeting APS Division of Fluid Dynamics Meeting Abstracts.
Aidun, Cyrus K., Clausen, J.R., 2010. Lattice-Boltzmann method for complex flows. Ann. Rev. Fluid Mech. 42 (1), 439–472.
Anagnostopoulos, P., Bearman, P.W., 1992. Response characteristics of a vortex-excited cylinder at low Reynolds numbers. J. Fluids Struct. 6 (1), 39–50.
Ansumali, S., Karlin IV, I.V., 2000. Stabilization of the lattice Boltzmann method by the H theorem: a numerical test. Phys. Rev. E Statis. Phys. Plasmas Fluids Related Interdis. Top. 62.6 Pt A, 7999–8003.
Blevins, R.D., Saunders, H., 1977. Flow-Induced Vibration. Van Nostrand Reinhold Co.
Bouzidi, M'Hamed, Firdaouss, M., Lallemand, P., 2001. Momentum transfer of a Boltzmann-lattice fluid with boundaries. Phys. Fluids 13 (11), 3452–3459.
Caiazzo, A., 2013. Analysis of lattice Boltzmann nodes initialisation in moving boundary problems. Prog. Comput. Fluid Dynam. Int. J. 8 (8), 3–10.
Chen, Y. et al., 2013. Momentum-exchange method in lattice Boltzmann simulations of particle-fluid interactions. Phys. Rev. E Statis. Nonlinear Soft Matter Phys. 88 (1), 013303.
Chen, Li et al., 2014. A comparative study of lattice Boltzmann methods using bounce-back schemes and immersed boundary ones for flow acoustic problems. Int. J. Numer. Methods Fluids 74 (6), 439–467.
Chen, S.S, Chung, H, 1976. Design guide for Calculating Hydrodynamic Mass. Part 1: Circular Cylindrical Structures. Nasa Sti/recon Technical Report N 77.
Chen, Shiyi, Doolen, G.D., 2012. Lattice Boltzmann method for fluid flows. Ann. Rev. Fluid Mech. 30 (1), 329–364.
Chen, Shoei Sheng, 1987. Flow-Induced Vibration of Circular Cylindrical Structures 63.
Dawson, S. Ponce, Chen, S., Doolen, G.D., 1993. Lattice Boltzmann computations for reaction-diffusion equations. J. Chem. Phys. 98 (2), 1514–1523.
De Rosis, Alessandro, Ubertini, S., Ubertini, F., 2014. A partitioned approach for two-dimensional fluid-structure interaction problems by a coupled lattice Boltzmann-finite element method with immersed boundary. J. Fluids Struct. 45 (1), 202–215.
De Rosis, Alessandro, Ubertini, S., Ubertini, F., 2014. A Comparison between the interpolated bounce-back scheme and the immersed boundary method to treat solid boundary conditions for laminar flows in the lattice Boltzmann framework. J. Sci. Comput. 61 (3), 477–489.
Delouei, A. Amiri et al., 2016. Non-Newtonian particulate flow simulation: a direct-forcing immersed boundary–lattice Boltzmann approach. Physica A Statistical Mechanics & Its Applications 447, 1–20.
Dettmer, W., Perić, D., 2006. A computational framework for fluid–rigid body interaction: finite element formulation and applications. Comput. Methods Appl. Mech. Eng. 195 (13–16), 1633–1666.
D'Humières, Dominique, 2002. Multiple–relaxation–time lattice Boltzmann models in three dimensions. Philosophical Transactions 360 (1792), 437.
Filippova, Olga, Hänel, D., 1998. Grid refinement for lattice-BGK models. J. Comput. Phys. 147 (1), 219–228.
Frisch, U., Hasslacher, B., Pomeau, Y., 1986. Lattice-gas automata for the Navier-Stokes equation. Phys. Rev. Lett. 56 (14), 1505.
Ginzburg, I., D'Humières, D., 2003. Multireflection boundary conditions for lattice Boltzmann models. Phys. Rev. E Statis. Nonlinear Soft Matter Phys. 68 (6 Pt 2), 066614.
Guo, Zhaoli, Zheng, C., Shi, B., 2002. An extrapolation method for boundary conditions in lattice Boltzmann method. Phys. Fluids 14 (6), 2007–2010.
Hassan, Marwan, Gerber, A., Omar, H., 2009. Numerical estimation of fluidelastic instability in tube arrays. J. Press. Vessel Technol. 132 (4), 269–278.
Hu, Junjie, Tao, S., Guo, Z., 2017. An efficient unified iterative scheme for moving boundaries in lattice Boltzmann method. Comput. Fluids 144, 34–43.
Inamuro, Takaji, 2012. Lattice Boltzmann methods for moving boundary flows. Fluid Dynam. Res. 44 (2), 24001–24021 (21).
Izquierdo, S., Fueyo, N., 2008. Characteristic nonreflecting boundary conditions for open boundaries in lattice Boltzmann methods. Phys. Rev. E Statis. Nonlinear Soft Matter Phys. 78 (2), 046707.
Ladd, Anthony J.C., 1993. Numerical simulations of particulate suspensions via a discretized Boltzmann equation. Part 1. Theoretical foundation. J. Fluid Mech. 271 (271), 285–309.
Lallemand, P., Luo, L.S., 2000. Theory of the lattice Boltzmann method: dispersion, dissipation, isotropy, Galilean invariance, and stability. Phys. Rev. E Statis. Phys. Plasmas Fluids Related Interdis. Top. 61.6 Pt A, 6546.
Lallemand, P., Luo, L.S., 2003. Theory of the lattice Boltzmann method: acoustic and thermal properties in two and three dimensions. Phys. Rev. E Statis. Nonlinear Soft Matter Phys. 68 (2), 036706.
Lallemand, Pierre, Luo, L.S., 2003. Lattice Boltzmann Method for Moving Boundaries. Academic Press Professional Inc..
Li, Huabing et al., 2004. Lattice Boltzmann simulation on particle suspensions in a two-dimensional symmetric stenotic artery. Phys. Rev. E Statis. Nonlinear Soft Matter Phys. 69 (3 Pt 1), 031919.
Li, Zho, Favier, J., D'Ortona, U., 2016. An immersed boundary-lattice Boltzmann method for single- and multi-component fluid flows. J. Comput. Phys. 304 (C), 424–440.
Luo, L.S. et al., 2011. Numerics of the lattice Boltzmann method: effects of collision models on the lattice Boltzmann simulations. Phys. Rev. E Statis. Nonlinear Soft Matter Phys. 83 (5 Pt 2), 056710.
Martínez, Daniel O., Chen, S., Matthaeus, W.H., 1994. Lattice Boltzmann magnetohydrodynamics. Physics of Plasmas 1 (6), 1850–1867.
Mei, Renwei et al., 2006. Consistent initial conditions for lattice Boltzmann simulations. Comput. Fluids 35 (8), 855–862.
Mei, Renwei, Shi, L.L., Shyy, A.W., 1999. An Accurate Curved Boundary Treatment in The Lattice Boltzmann Method. Institute for Computer Applications in Science and Engineering (ICASE).
Mittal, S., Tezduyar, T.E., 2010. A finite element study of incompressible flows past oscillating cylinders and aerofoils. Int. J. Numer. Methods Fluids 15 (9), 1073–1118.
Peng, Cheng et al., 2016. Implementation issues and benchmarking of lattice Boltzmann method for moving rigid particle simulations in a viscous flow. Comput. Math. Appl. 72 (2), 349–374.
Roshko, A., 1954. On The Development of Turbulent Wakes from Vortex Streets. Technical Report Archive & Image Library.
Takashi, Nomura, 1994. ALE finite element computations of fluid-structure interaction problems. Comput. Methods Appl. Mech. Eng. 112 (4), 291–308.
Takashi, T., Nomura, Hughes, T.J.R., 1992. An arbitrary Lagrangian-Eulerian finite element method for interaction of fluid and a rigid body. Comput. Methods Appl. Mech. Eng. 95 (1), 115–138.
Tanaka, H. et al., 2002. Fluidelastic analysis of tube bundle vibration in cross-flow. J. Fluids Struct. 16 (1), 93–112.
Tao, Shi, Hu, J., Guo, Z., 2016. An investigation on momentum exchange methods and refilling algorithms for lattice Boltzmann simulation of particulate flows. Comput. Fluids 133, 1–14.
Wang, Y. et al., 2016. On the immersed boundary-lattice Boltzmann simulations of incompressible flows with freely moving objects. Int. J. Numer. Methods Fluids.
Wen, Binghai et al., 2014. Galilean invariant fluid–solid interfacial dynamics in lattice Boltzmann simulations. J. Comput. Phys. 266 (4), 161–170.
Wu, J., Shu, C., 2009. Implicit velocity correction-based immersed boundary-lattice Boltzmann method and its applications. J. Comput. Phys. 228 (6), 1963–1979.
Yang, X., Zhang, X., Li, Z., He, G.W., 2009. A smoothing technique for discrete delta functions with application to immersed boundary method in moving boundary simulations. J. Comput. Phys. 228 (20), 7821–7836.